

Dynamic Study of Tunable Stiffness Scanning Microscope Probe

by

Myraida Angélica Vega González

Submitted to the Department of Mechanical Engineering in Partial  
Fulfillment of the Requirements for the Degree of

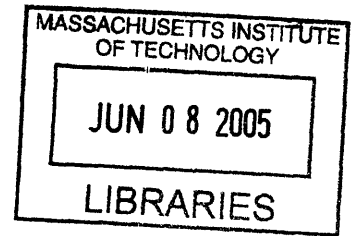
Bachelor of Science

at the

MASSACHUSETTS INSTITUTE OF TECHNOLOGY

June 2005

© 2005 Myraida A. Vega  
All Rights Reserved



The author hereby grants to MIT permission to reproduce and to  
distribute publicly paper and electronic copies of this thesis  
document in whole or in part.

Signature of Author.....  
Department of Mechanical Engineering  
May 6, 2005

Certified by .....  
Sang-Gook Kim  
Associate Professor of Mechanical Engineering  
Thesis Supervisor

Accepted by .....  
Ernest G. Cravalho  
Professor of Mechanical Engineering  
Chairman, Undergraduate Thesis Committee

**ARCHIVES**

# Dynamic Study of Tunable Stiffness Scanning Microscope Probe

by

Myraida Angélica Vega González

Submitted to the Department of Mechanical Engineering on  
May 6, 2005 in Partial Fulfillment of the Requirements for the  
Degree of Bachelor of Science in Mechanical Engineering

## ABSTRACT

This study examines the dynamic characteristics of the in-plane tunable stiffness scanning microscope probe for an atomic force microscope (AFM). The analysis was carried out using finite element analysis (FEA) methods for the micro scale device and its macro scale counterpart, which was designed specifically for this study. Experimental system identification testing using sound wave and high-speed camera recordings was done on the macro scale version to identify trends that were then verified in the micro scale predictions.

The results for the micro scale device followed the trends predicted by the macro scale experimental data. The natural frequencies of the device corresponded to the three normal directions of motion, in ascending order from the vertical direction, the out-of-plane direction, and the horizontal direction. The numerical values for these frequencies in the micro scale are 81.314 kHz, 51.438 kHz, and 54.899 kHz for the X, Y, and Z directions of vibration respectively. The error associated with these measurements is 6.6% and is attributed to the high tolerance necessary for measurements in the micro scale, which was not matched by the macro scale data acquisition methods that predict the natural frequency range.

The vertical vibrations are therefore the limiting factor in the scanning speed of the probe across a sample surface, thus requiring the AFM to scan at an effective frequency of less than 81.3 kHz to avoid resonance.

Thesis Supervisor: Sang-Gook Kim  
Title: Associate Professor of Mechanical Engineering

## Table of Contents

1.0 Introduction	5
2.0 Modeling Dynamic Properties of the In-plane AFM Probe	10
2.1 Atomic Force Microscope	10
2.2 Dynamic System Identification	11
2.2.1 Modal Analysis	11
2.2.2 Lumped Stiffness Model	13
2.2.3 High Speed Video Capture	16
2.2.4 Fast Fourier Transform	16
3.0 Experimental Setup	18
3.1 Finite Element Analysis: ANSYS	18
3.1.1 Apparatus	18
3.1.2 Procedure	18
3.2 Macro Model Experiment	19
3.2.1 Apparatus	20
3.2.2 Procedure	20
4.0 Results	22
5.0 Discussion	27
6.0 Conclusion	29
References	31
Appendices	
A1 ANSYS Code	32
A2 ANSYS Outputs: Mode Shapes	34
A3 MATLAB Code	36
A4 Experimental Outputs (Raw Data)	39

## Table of Figures

1. Conventional Atomic Force Microscope Schematic	5
2. Tunable Stiffness Atomic Force Microscope Probe	7
3. Device design with major components labeled	8
4. Unreleased in-plane AFM probe with electrical connections on the surface for the electrostatic actuators which engage the clutches	9
5. Horizontal Deflection of an Atomic Force Microscope Tip	10
6. Flexure 1 parameters and its lumped stiffness model	14
7. Flexure 2 parameters and its lumped stiffness model	15
8. Flexure 3 parameters and its lumped stiffness model	15
9. Experimental setup for the macro scale device dynamic system ID	20
10. Mode Shapes as plotted by ANSYS for the Micro Device in the Engaged and Unengaged Settings	22
11. Results Summary: Macro Device-Unengaged	25
12. Results Summary: Micro Device-Unengaged	25
13. Results Summary: Macro Device-Engaged	26
14. Results Summary: Micro Device-Engaged	26
15. Experimental Setup Schematic for Full Dynamic Spectrum Testing	30

## 1.0 Introduction

Atomic Force Microscopy is utilized in a wide range of technologies affecting the electronics, telecommunications, biological, chemical, automotive, aerospace and energy industries. An atomic force microscope (AFM) can not only image surfaces at atomic resolution but it can also measure force at the subnano-Newton scale. Atomic force microscopy is a specifically powerful technique with a wide range of applications in biology, allowing not only for imaging but also for different types of probing and manipulation at the nanometric scale.

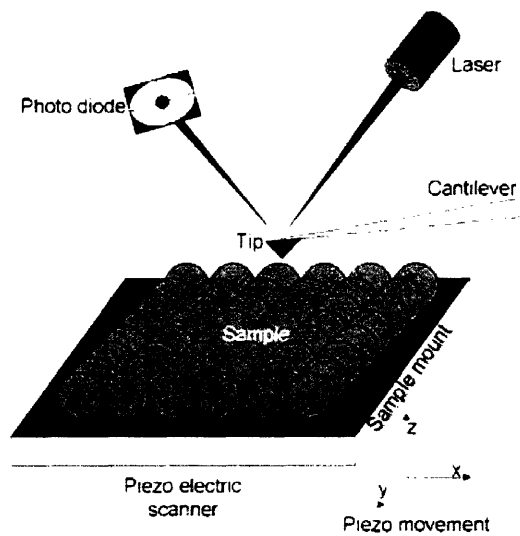


**Figure 1:** Conventional Atomic Force Microscope Schematic [1]

A conventional atomic force microscope, like the one in **Figure 1** above, consists of an atomically sharp tip (usually no more than  $5\mu\text{m}$  in length) attached to a micro-cantilever. The cantilever is outfitted with feedback mechanisms that allow the piezoelectric actuators to maintain the tip at a constant force (when interested in height readings) or constant height (when acquiring force readings) above the sample surface. As the AFM tip scans the surface of the sample, moving up and down with the contour of the surface, a laser beam focused onto the top of the cantilever is deflected off into a dual element photodiode. Data is accumulated by measuring the deflection of the cantilever as the tip scans the sample. The data from the detection system is then turned into force readings

using the displacement measurements and the known stiffness of the cantilever. The force between the tip and the sample surface is very small, usually in the nano-Newton scale.

The primary purpose of these instruments is to quantitatively measure surface morphology and construct three dimensional topographical maps of the surface by plotting the local sample height vs. the horizontal probe tip position. These height measurements are customarily taken with a constant force applied to the surface. The stiffness of the cantilever, therefore, plays a large role as to the performance of the AFM itself. Atomic force microscopy is one of the most powerful tools for determining the surface topography of native biomolecules at sub-nanometer resolution; the AFM allows biomolecules to be imaged not only under physiological conditions, but also while biological processes are at work. One rapidly evolving area in scanning force microscopy is the construction of tips to measure specific force interactions in cells. [4]

The purpose of this study is to investigate the dynamic properties of an in-plane tunable stiffness AFM probe. The problem it addresses is the fact that, during biological scans of cells, the cantilever stiffness became a source of concern when multiple hardness objects within the cell were being studied in the same scan. As the tip moves from a hard surface to a soft membrane (or vice versa), the force is kept at a constant value (as is customary for height readings) so the subsequent pressure applied to the surface is no longer optimal for the soft membrane. This requires switching probes during a scan, consequently losing continuity and precision. By designing a probe whose stiffness can be switched, the force applied to each different surface can be optimized without disrupting the scan. With this design, shown in **Figure 2**, the probe stiffness can be adapted by engaging or disengaging flexures when the tip goes from one surface to another, resulting in an order of magnitude stiffness change between the engaged position and the unengaged position.

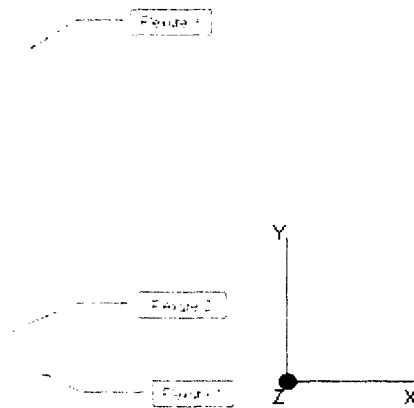


**Figure 2:** Tunable Stiffness Atomic Force Microscope Probe (Flexure labels will remain the same throughout the remainder of this paper). [3]

Actuation and sensing in the z-direction can easily be integrated into this coplanar MEMS structure. A single strand carbon nanotube (MWNT) is used as a high-aspect-ratio tip. The inherent capability of the in-plane AFM probe for building a massively parallel array is an important feature of the design with a great impact on the productivity of the AFM scanning process. The in-plane structure also enables possible integration of micro-fluidic channels for reagent delivery and nanopipetting, photonic channels and electronic wiring. [3]

The acquisition of data with this new design differs slightly from the conventional methods described earlier, if only in the actual details of operation. The displacement is still measured using a closed control loop, but it now consists of a capacitive sensor and a combdrive actuator that maintain a constant force between the tip and the sample surface. When the surface hardness increases, Flexure 2 in **Figure 2** is engaged by applying a voltage to the two electrostatic actuators that engage the clutches. **Figure 3** shows the full device design with all these components labeled.

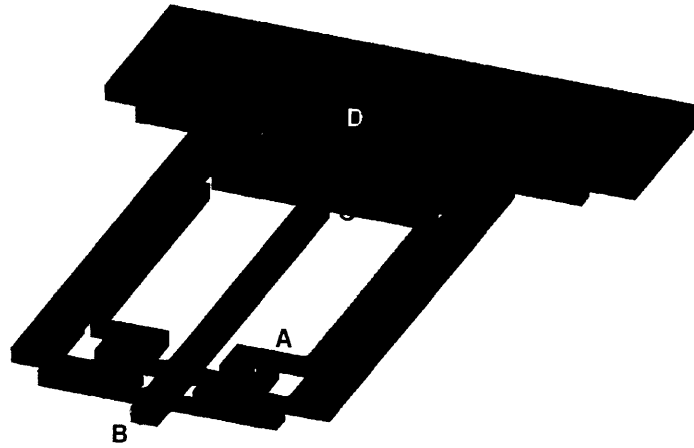


**Figure 3:** Device design with major components labeled (**A:** Electrostatic clutch, **B:** High-aspect-ratio carbon nanotube tip, **C:** Capacitive sensor, **D:** Combdrive actuator). [3]

This new design poses some design challenges. The vertical motion of the tip is now bounded by two (or three if the probe is engaged) flexures attached to a vertical cantilever. The length of this cantilever now acts as the effective length of the tip itself and is around twenty times as long as conventional probes. Because of this increase in length, it is imperative to conduct a dynamic analysis since the resonant frequencies and harmonic modes will have a discernible effect on the performance of this probe. The horizontal and out-of-plane vibrations of this lengthy cantilever need to be studied in order to fully understand the limitations of this design and to be able to assess the potential applications of it. These challenges are magnified by the scale of the device, which can be fully appreciated in **Figure 4**. The tolerances needed for an exact characterization of the probe are small enough to warrant extensive consideration during the error analysis that follows the data acquisition.

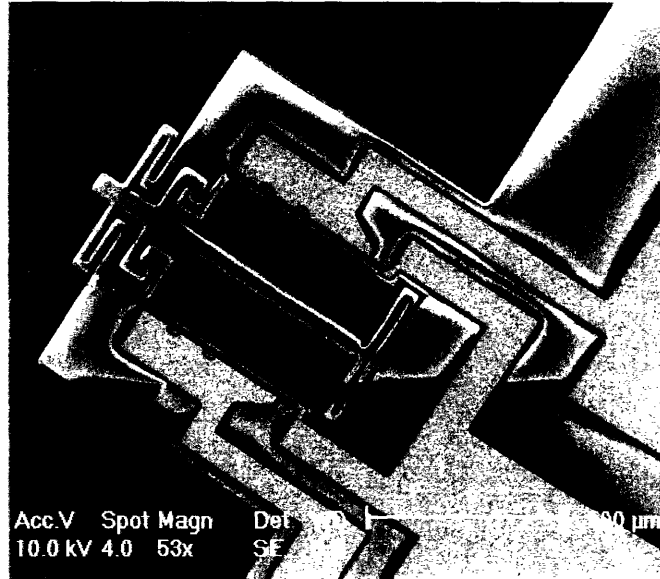


**Figure 4:** Unreleased in-plane AFM probe with electrical connections on the surface for the electrostatic actuators which engage the clutches.[3]

The expected outcome of the system identification of this probe are that the natural frequency in the vertical direction will be the limiting factor for the maximum scanning speed of the probe, followed by the out of plane direction vibrations and lastly, the horizontal direction harmonic. The natural frequencies are of great interest since the tip motion while scanning a surface will induce a harmonic-like oscillation. If this movement is near the natural frequencies of the device, the probe will begin to show signs of resonance which will render any data acquired to be less meaningful or will damage the probe and the scanned surface. By studying the AFM probe's dynamic characteristics, the resonance range can be avoided by selecting the proper scanning speed of the device. This will therefore limit the range of the probe to scans where the settings dictated by the dynamic identification are optimal.

The thesis studies the harmonic resonance frequencies of the tunable stiffness probe design, which will limit the scanning speed of the probe. This data will help determine the maximum resolution of the probe, the optimal use of the design, and ultimately to make better designs of the scanning probe system.

## 2.0 Modeling Dynamic Properties of the In-plane AFM Probe

### 2.1 Out of Plane Motion of an Atomic Force Microscope

An AFM works by measuring the vertical motion of the cantilever support when the tip scans a sample surface. This method of data acquisition assumes that the tip motion in the horizontal and out-of-plane directions depends on the sine of the deflection angle in these directions and thus makes negligible errors in the vertical direction, as seen in **Figure 5**.

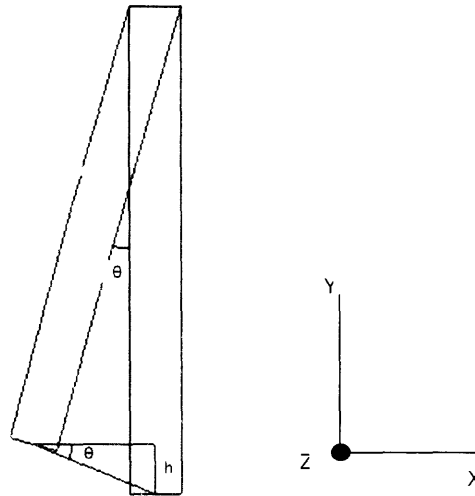


**Figure 5:** Horizontal deflection of an AFM probe tip, the angle of deflection corresponds to the angle associated with the vertical displacement.

In the above figure, a horizontal deflection making an angle  $\theta$  with the resting position of the probe corresponds to a height reading of  $h$ . For a conventional AFM scan, this height  $h$  is negligible compared to the pure vertical motion of the tip corresponding to the actual sample topography. In the present design, however, since the effective length of the tip has been substantially increased, the corresponding vertical displacement contribution from the horizontal and out-of-plane directions become significant. Because of this, the dynamic characteristics, including the resonant frequencies, in the two horizontal directions are studied for the tunable stiffness probe design.

## 2.2 Dynamic System Identification

The main purpose of this study is to define the dynamic characteristics of the in-plane AFM probe device. There are several different methods to do this and both the theoretical and experimental methods were chosen to have better reliability and ease of implementation. By having four different data sets, each of them estimating the natural frequency of the device in multiple stiffness settings, a consistent model can be made and reliable predictions derived. The four chosen approaches for system identification are: modal analysis using finite elements, lumped stiffness approximation derived from theory, high speed video capture of the vibrating device, and Fast Fourier Transform from a sound recording. The latter two experimental methods were done with a macro-scale version of the device manufactured specifically for this experiment. This measured data was then scaled accordingly. Each of these approaches is described below.

### 2.2.1 Modal Analysis

Modal Analysis is used to determine the vibrational characteristics (natural frequencies and mode shapes) of a structure. The basic dynamic characteristics of the device can be measured later and any changes in the design may be assessed and scaled accordingly. This is the reason why this analysis was chosen over more detailed dynamic analyses such as transient dynamic, harmonic response or spectrum analysis.

Before starting a modal analysis, there are a number of assumptions that must be made. These assumptions are that the device has constant stiffness and mass effects, there is no damping during the motion, and the structure is in free vibration mode. If these assumptions hold true then the modal analysis gives the correct natural frequency and modal shape of the device being studied.

The driving equation in this analysis is the equation of motion for an undamped system which, in matrix notation, is:

$$[M]\{\ddot{u}\} + [K]\{u\} = \{0\} \quad (1)$$

where  $[M]$  is the mass matrix,  $[K]$  is the stiffness matrix (assumed to be constant in all directions for the present analysis), and  $\left\{ \ddot{u} \right\}$ ,  $\{u\}$  are the acceleration and displacement vectors respectively.

For a linear system, like the present analysis assumes this one is, the free vibrations will be harmonic and follow the form:

$$\{u\} = \{\Phi\}_i \cos \omega_i t \quad (2)$$

where  $\{\Phi\}_i$  is the eigenvector representing the mode shape of the  $i^{th}$  natural frequency,  $\omega_i$  is the  $i^{th}$  natural frequency, and  $t$  is time.

Thus, substituting **Eq. 2** into **Eq. 1** gives the equation of motion as:

$$\left( -\omega_i^2 [M] + [K] \right) \{\Phi\}_i = \{0\} \quad (3)$$

whose trivial solution is of course  $\{\Phi\}_i = \{0\}$  and its non-trivial solution is the determinant of the terms in parenthesis, i.e.:

$$\left| ([K] - \omega^2 [M]) \right| = 0 \quad (4)$$

This solution is an eigenvalue problem [5] which may be solved for up to  $n$  values of  $\omega^2$  and  $n$  eigenvectors  $\{\Phi\}_i$  which satisfy **Eq. 3** ( $n$  being the number of degrees of freedom defined in the model).

The natural frequencies that are calculated by this analysis carry units of radians per unit time. The natural frequencies, in Hz, of the device can be found using the simple conversion:

$$f_i = \frac{\omega_i}{2\pi} \quad (5)$$

where  $f_i$  is the  $i^{th}$  natural frequency in cycles per unit time.

The modal analysis is easily extended to a mass distribution study of the device, which in the present situation is imperative. The effective mass for each of the mode shapes must be calculated since the structure is constrained in such a way that the total mass is not fully present in the vibration [5]. The mass that corresponds to each mode shape is dependent on the participation factor ( $\gamma_i$ ) for each excitation direction. This participation factor is defined as:

$$\gamma_i = \{Y\}'_i [M] \{D\} \quad (6)$$

where  $\{D\}$  is the vector describing the excitation direction and  $\{\Phi\}'_i$  is the normalized eigenvector defined as:

$$\{\Phi\}'_i [M] \{\Phi\}_i = 1 \quad (7)$$

The effective mass for the  $i^{th}$  mode (also a function of the excitation direction) is:

$$M_{ei} = \frac{\gamma_i^2}{\{Y\}'_i [M] \{Y\}_i} \quad (8)$$

These effective masses are used as the mass matrix for the correlation between the experimental data and the FEA analysis models.

### 2.2.2 Lumped Stiffness Model

Another way of acquiring the natural frequency of the device is using a lumped stiffness model. According to **Eq. 4**, the natural frequency of the structure will be in the form:

$$\omega = \sqrt{\frac{k}{m}} \quad (9)$$

where  $k$  can be determined geometrically by using a lumped stiff beam approximation for each state of the device. With this simple formula, it is possible to derive a close estimate

of the natural frequency of the device by simply knowing its material properties and geometry.

The stiffness for one beam with length  $L$ , width  $w$  and thickness  $t$  can be calculated using:

$$k_{beam} = \frac{12EI}{L^3} \quad (10)$$

where  $E$  is the Young's modulus and  $I$  is the moment of inertia of the beam, defined as:

$$I = \frac{wt^3}{12} \quad (11)$$

The lumped stiffness of Flexure 1 in **Figure 2**, is then:

$$k_1 = 2 \frac{Ewt_1^3}{L^3 + 2L_1^3} \quad (12)$$

where the length parameters are defined as shown in **Figure 6**.

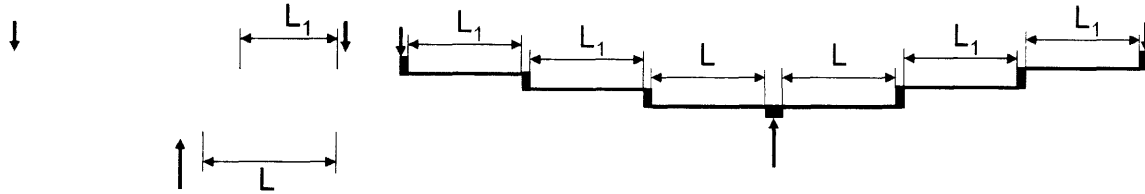


**Figure 6:** Flexure 1 length parameters and its lumped stiffness model. it is assumed that the vertical beams connecting the horizontal cantilevers are stiff (they do not deform during the AFM motion) and that the forces felt are solely in the Y-direction. [2]

The lumped stiffness of Flexure 2 in **Figure 2**, is:

$$k_2 = 2 \frac{Ewt_2^3}{L_2^3} \quad (13)$$

where the length parameters are defined as shown in **Figure 7**.

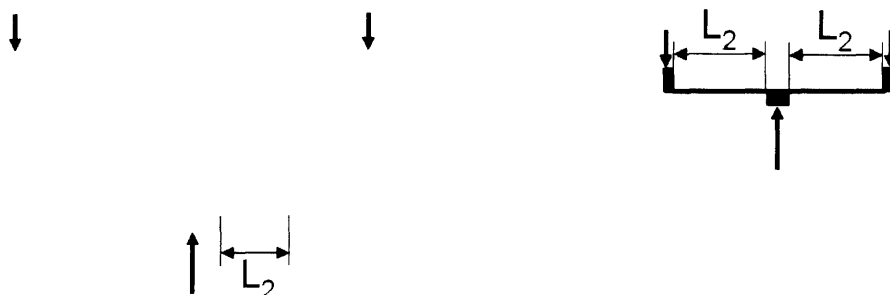


**Figure 7:** Flexure 2 parameters and its lumped stiffness model, it is again assumed that the forces are solely in the Y-direction and that the connections between the cantilevers are stiff. [2]

The lumped stiffness of Flexure 3 in **Figure 2**, is:

$$k_3 = \frac{Ewt_3^3}{L_3^3} \quad (14)$$

where the length parameters are defined as shown in **Figure 8**.

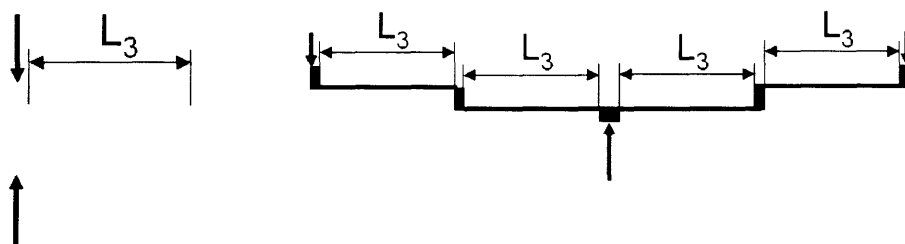


**Figure 8:** Flexure 3 parameters and its lumped stiffness model, assuming that the force is solely in the vertical direction and the connecting vertical beams are stiff throughout the motion. [2]

Using these lumped stiffness models, the natural frequencies of each of the two settings (engaged and unengaged) can be calculated using **Eq. 9** where:

$$\omega_{unengaged} = \sqrt{\frac{k_1 + k_3}{m}} \quad (15)$$

and

$$\omega_{engaged} = \sqrt{\frac{k_1 + k_2 + k_3}{m}} \quad (16)$$

This geometrical approximation method [2], is used to estimate a frequency range where the modal analysis outputs will likely lie. The error that stems from this analysis is expected to stem from the mass term in **Equations 15 and 16** since the initial mass

chosen for these equations will be the total mass of the system, not the effective mass in each direction.

### 2.2.3 High Speed Video Capture

The third method used to derive the natural frequency of the device was using a high speed camera to record the motion of the device after a force was applied to Flexure 1. The video was then analyzed and the natural frequency calculated using the simplest definition of natural frequency [5], namely:

$$\omega = \frac{\text{cycles}}{\text{unit\_time}} \quad (17)$$

### 2.2.4 Fast Fourier Transform

The Fast Fourier Transform (FFT) algorithm is a much faster method for computing the Discrete Fourier Transform (DFT) for all the harmonics of a given problem [6]. The DFT is expressed, via Euler's identity as:

$$\alpha e^{i\alpha} = \alpha \cos \alpha + i\alpha \sin \alpha \quad (18)$$

where  $\theta$  is the phase between the input signal (in this case a recorded sound wave),  $x_c$ , and the sampled signal,  $x_r$ , [7] which is defined as:

$$x_r = x_c(i\Delta t) \quad (19)$$

The  $\alpha$  term in **Eq. 18** is defined by:

$$\alpha(m) = 2\sqrt{Cor_{\sin}(m)^2 + Cor_{\cos}(m)^2} \quad (20)$$

where  $m$  is the harmonic being calculated and  $Cor_{\sin}, Cor_{\cos}$  are the correlations associated with the harmonics [8] which are in turn defined by:

$$Cor_{\sin}(m) = \frac{1}{n} \sum_{i=1}^n x_r \sin(i \Delta t \Delta m \Delta v_r) \quad (21)$$

and

$$Cor_{\cos}(m) = \frac{1}{n} \sum_{i=1}^n x_i \cos(i \Delta t \Delta m \Delta w_f) \quad (22)$$

where  $w_f$  is the fundamental frequency calculated using:

$$w_f = \frac{2\pi}{n\pi t} \quad (23)$$

Evaluating a signal using this approach can be time consuming and redundant. For instance, all of the sine probes are zero at the start and the middle of the recording, so there's no need to perform operations for them. Further, all even-numbered sine probes cross zero at  $\frac{1}{4}$  increments through the record, every fourth probe at  $\frac{1}{8}$  and so on. The power of two in this pattern is obvious, and the FFT exploits this by requiring a power of two transform, and splitting the process into cascading groups of two. Similarly, there are patterns for when the sine and cosine are 1.0, and multiplication is not needed. By exploiting these redundancies, the savings of the FFT over the DFT are immense. While the DFT needs  $O(n^2)$  arithmetical operations, an FFT will compute the same result in only  $O(n \log n)$  operations. [9] This means that, for a 1500 point FT, an FFT will need 4,764 operations, compared to the 2,250,000 needed by the DFT.

For these reasons, the FFT algorithm was chosen to study the sound data acquired through experiment.

### 3.0 Simulation and Experimental Setup

The experimental data acquired in this study can be divided into two major categories: computational modeling using FEA and a physical experimental setup using a macro scale version device. These two methods are described below.

#### 3.1 Finite Element Analysis: ANSYS

The first analyses were finite element analysis models which were then studied to acquire the necessary data, i.e. the natural frequency. This process was completely computational and is detailed in the following sections.

##### 3.1.1 Apparatus

This method required the FEA computational program ANSYS Version 8.1.

##### 3.1.2 Procedure

The finite element analysis (FEA) program ANSYS was used to run modal analyses on both the macro and micro versions of the device. Solid models of the devices were imported into the program as .IGS files and then their material properties were defined in order to run the simulation. The code of these simulations can be found in **Appendix A1**.

The modal analysis option treats all elements as linear and it is necessary to input the Young's modulus, density, and the Poisson's ratio of the material to be used. For the present device, the values for these constants were:

**Table 1:** Material constants for the macro and micro versions of the probe as defined for the ANSYS simulations.

	Young's Modulus [GPa]	Density $\left[ \frac{kg}{m^3} \right]$	Poisson's Ratio
<b>Macro version (Polycarbonate)</b>	2.7	1200	0.42
<b>Micro version (SU-8)</b>	4.02	1200	0.22

After defining the imported models as solids (solid – tet - 10node 92) and then defining their material characteristics as described in **Table 1**, the mesh was produced using ANSYS's 'Mesh Tool'. The mesh was created using tetrahedron mesh elements defined with the 'smart size' option set at 6 for the micro devices and at 4 for the macro devices. The next step in the preprocessor was to define the constraints. All degrees of freedom were constrained at the non-vibrating walls of the device. This ended the preprocessor commands and the program was ready to enter the solver.

The solver was set to 'Modal Analysis – Block Lanczos', which is the default setting for modal analysis. The number of modes to extract was set to 10 and the frequencies to sweep were set to 1Hz-10 kHz for the micro devices and 0 Hz to 250 Hz for the macro devices, suitable ranges chosen after calculating the expected natural frequencies using the method described in **Section 2.2.2**. These are the last parameters that need to be specified, everything else was left as the default values. The simulation is ready to be solved at this point, and the results acquired using this method will be presented and discussed in **Section 4**.

### **3.2 Macro Model Experiment**

The second stage of the experimental determination of the natural frequency was performed using a macro scale mockup of the device. This setup allowed simultaneous data acquisition via two different mediums: a high speed camera that recorded the motion and a microphone to record the sound waves generated by the vibrations. These data sets are then compared to the values acquired through FEA and using the lumped stiffness theory.

### 3.2.1 Apparatus

The experimental setup used for this experiment is represented by the following diagram:

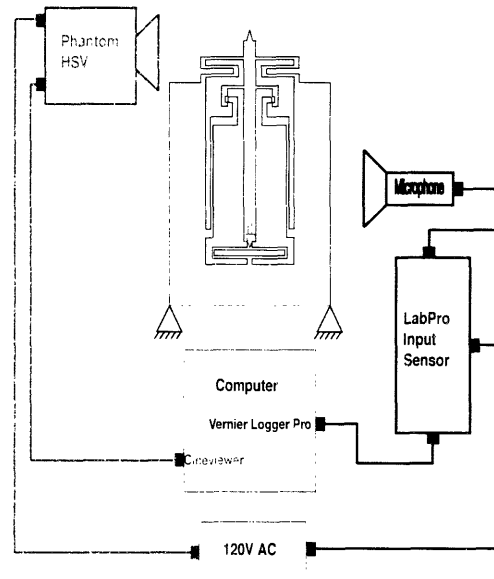


**Figure 9:** Experimental setup for the macro scale device dynamic system identification

The microphone was attached to a LabPro sensor which recorded the data into VERNIER software's LoggerPRO program. The sampling rate was set to 5 kHz per second and data was recorded for 1 second. The Nyquist frequency for this setup was 2.5 kHz.

The high speed video camera was a Phantom HSV camera which recorded the motion and was linked to the PHANTOM Capture program. The resolution was set to 1024x256 pixels and the sampling rate was set to 4200 frames per second with an exposure increment of 238 $\mu$ s. The Nyquist frequency for this method was therefore 2.1 kHz.

### 3.2.2 Procedure

The device was agitated by plucking the Flexure 1 downwards. The data acquisition was started simultaneously in order to record the subsequent vibration. The sound data was then analyzed using the LoggerPRO program to output an FFT plot. The plot served as an immediate visual check for the natural frequency values since it is trivial to estimate the

range in which they are located. Further study of the numerical data associated with the plot gave exact values for the natural frequencies in the directions of interest.

The video files were analyzed by defining an origin on the screen and measuring the time increment for the device to complete one full cycle of vibration. These measurements were then put into a MATLAB script that calculated the error associated with the video data's tolerance (since it only takes a sample every 238  $\mu\text{s}$ , the values read are really  $\pm 119 \mu\text{s}$ ) along with the average and standard deviation of the video data. The script, which makes up **Appendix A3**, also plotted the results associated with the data manipulation. A summary of these results is presented in the following section.

## 4.0 Results

The experimental methods described above looked to find the natural frequency of the macro device, which would then serve as a check for the micro device's dynamic identification. In the present section, a summary of the data acquired from all these methods is presented for both the macro and micro devices in the unengaged and engaged settings. The complete collection of Phantom camera output plots, as well as the sound output's FFT plots for each of the device settings are presented in **Appendix A4**.

The complete collection of ANSYS outputs is presented in **Appendix A2**. Mode shape plots for the three main directions of vibration are presented below in **Figure 10**.

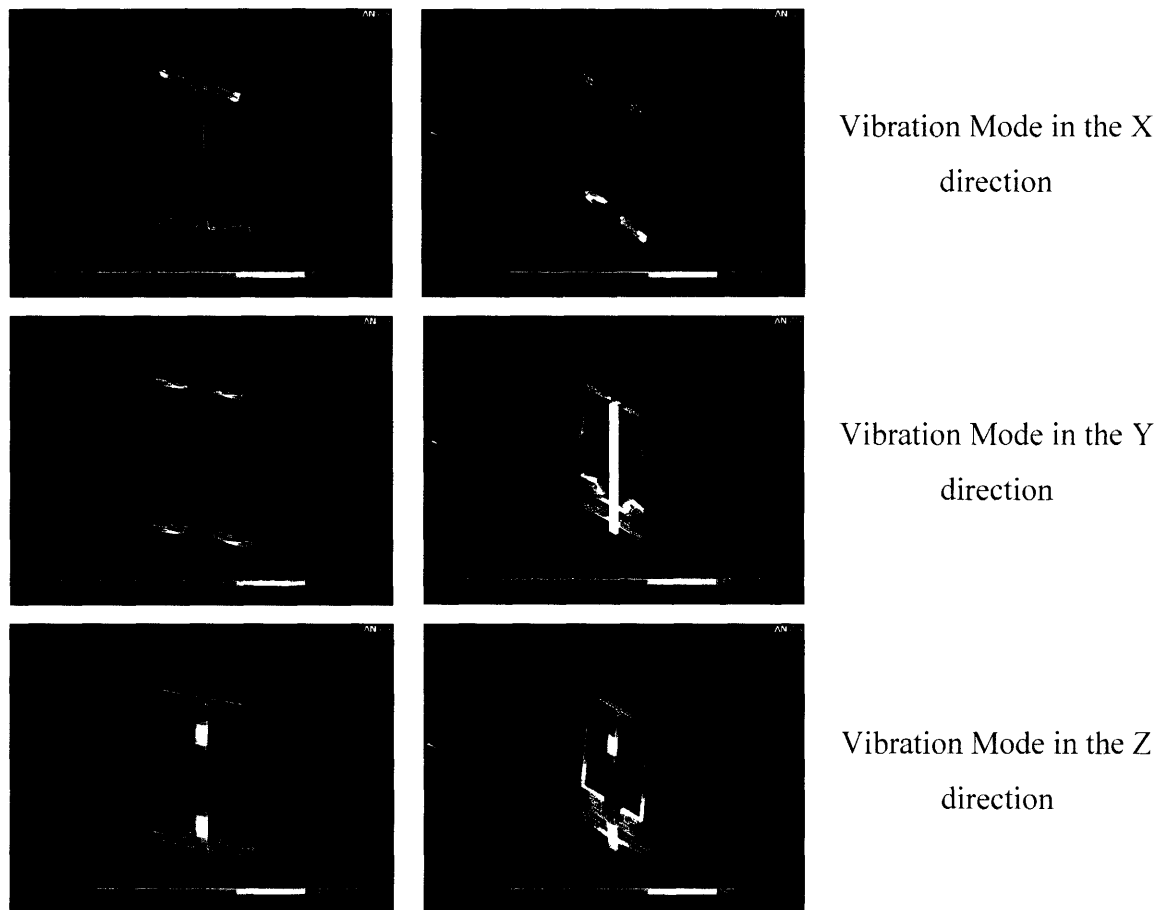


**Figure 10:** Mode Shapes as plotted by ANSYS for the Micro Device in the Engaged and Unengaged Settings.

As seen in **Figure 10**, there are harmonics in the frequency spectrum that exhibit vibration in only one direction of motion. This is clear in the previous plots, but further confidence in this statement is gained once the ANSYS Output window is studied, since the participation factor ( $\gamma_i$ ) is listed as 1.0 for these directions. Realizing that this corresponds to a vibration in the specific direction of interest, ANSYS therefore predicts the effective mass fraction for the particular motion as well as the natural frequency in the X, Y, and Z directions. This is the natural frequency that is taken as the theoretically predicted natural frequency in the subsequent plots.

The experimental data acquired for the macro device through the sound measurement generated the whole frequency spectrum associated with the tunable probe in each setting. The natural frequencies associated with each direction of vibration were therefore measured for both the unengaged and engaged settings. They were then compared to the theoretical predictions of these frequencies that were calculated using ANSYS. The numerical data is presented in **Table 2** below, and the raw data is attached as **Appendix A4**.

**Table 2:** Macro device's natural frequencies in the three normal directions of motion [Hz]

	<b>X (horizontal)</b>	<b>Y (vertical)</b>	<b>Z (out-of-plane)</b>
<b>Experimental</b>	671.97±174	125.46±6.27	385±59.3
<b>FEA (ANSYS)</b>	487.07	149.55	371.72
<b>Error</b>	27.5%	19.2%	3.5%

The error that is calculated for each of these frequencies is the error associated with the average value of the natural frequency in each direction. It is clear from this data that the vertical harmonic oscillations will drive the constraints in the design, and will therefore be the most interesting to study. It is worth noting that this trend is also present in the micro version of the probe, and the natural frequencies associated with the micro scale probe in the X, Y, and Z directions of motion are 81.314 kHz, 51.438 kHz, and 54.899 kHz respectively. The following discussion deals exclusively with the vertical vibrations of both the macro and micro versions of the device in more detail.

There were a total of five data sets acquired for the macro device, numbered in the plots according to the definitions presented in **Table 3**. The micro device, however, only has three data sets associated with it since experimental natural frequencies were not gathered. The following discussion addresses the natural frequency in the vertical direction, since it was found to be the limiting frequency for the performance of the device and was therefore studied in further detail.

**Table 3:** Definition of the ‘Data Set Number’ used as X-axis on Figures 11-14

	<b>Data Set Number</b>				
	<b>1</b>	<b>2</b>	<b>3</b>	<b>4</b>	<b>5</b>
<b>Macro Device</b>	Theory: Total Mass	Theory: Mass Fraction	FEA	Experimental: Camera	Experimental: Sound
<b>Micro Device</b>	Theory: Total Mass	Theory: Mass Fraction	FEA	n/a	

The first number in the series corresponds to the Lumped Stiffness theory described in **Section 2.2.2**. This particular approach takes into consideration the mass of the system as a whole, not the mass that is being acted upon by the flexures. Because of this, solid models of each device setting were imported into ProEngineer and the effective mass was calculated in much the same way as ANSYS did for the FEA analysis. Data set 2 corresponds to the Lumped Stiffness theory with the effective mass correction. The third data set corresponds to ANSYS’s predictions for the natural frequencies using modal analysis, effectively going through the method presented in **Section 2.2.1**. The last two data sets, which only appear for the macro device settings, correspond to the experimental setup and are an average of the raw data gathered during each experimental run for the two active sensors.

Below, the results summary for each device setting, in both macro and micro scale, is presented graphically with their corresponding average and standard deviations. The summary plots the natural frequency acquired through each different method of dynamic identification as a separate marker.

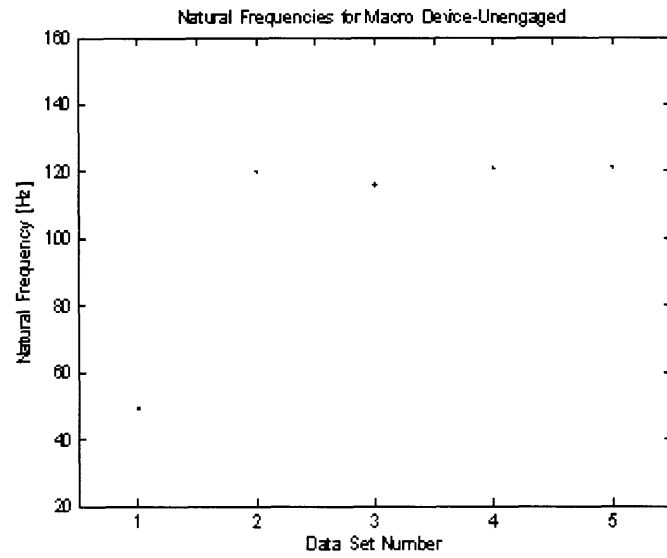


**Figure 11: Results Summary: Macro Device-Unengaged**

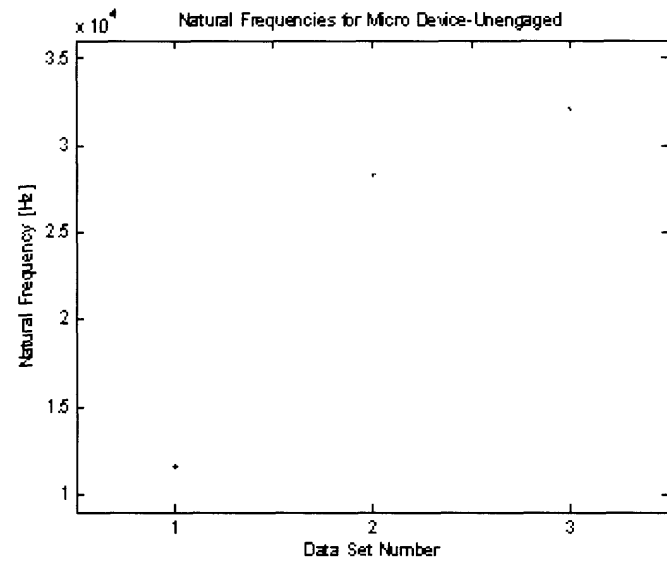


**Figure 12: Results Summary: Micro Device-Unengaged**

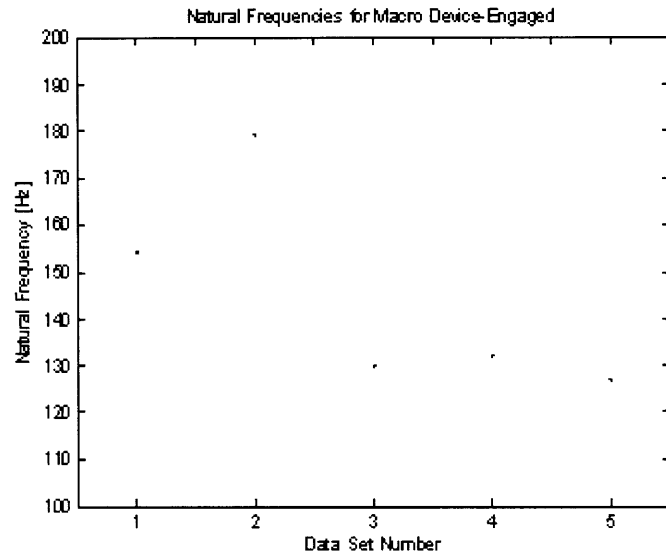


**Figure 13:** Results Summary: Macro Device-Engaged

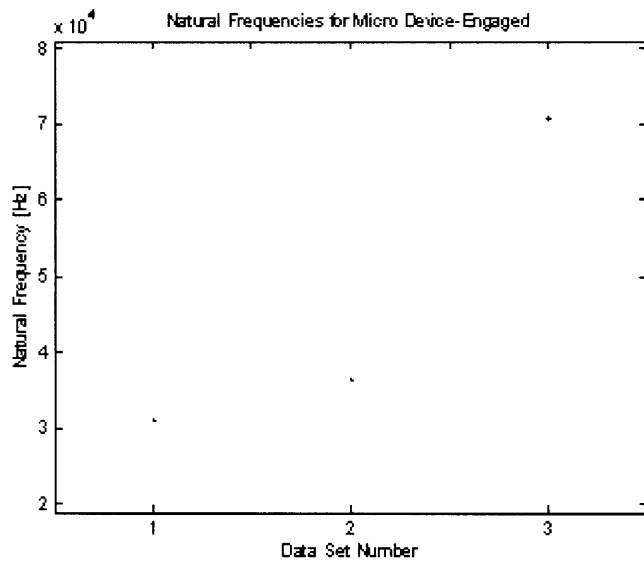


**Figure 14:** Results Summary: Micro Device-Engaged

## 5.0 Discussion

The data gathered from the different methods is very specific to each approach used. For the discussion of this data, which is concerned solely with the vibration in the vertical direction, the 'unengaged' setting will be discussed first followed by the discussion of the 'engaged' setting.

From **Figure 11** it is clear that the different methods converge to a specific range once the mass correction is introduced to the lumped stiffness model. The natural frequency in the vertical direction for the unengaged macro device is, once data set 1 is disregarded as an outlier, around  $120 \pm 2.4$  Hz. The natural frequency for the micro device is not as obvious as for the macro device. Once again disregarding the first data set, the natural frequency in the vertical direction is around  $30 \pm 2.7$  kHz. This data has a larger dispersion among its data points and would therefore seem to be less reliable. Upon further study, the fact that the scale of the two devices is almost 200:1 gives the impression that the tolerances associated with the two scales are different enough so that the standard deviation shown by the micro device is acceptable for this study. A difference of merely a few microns would produce a significant jump in the micro scale data whereas the macro device is more forgiving. The micro data is also reliable since the manipulations are straight calculations using FEA, not a scaling down of macro data, which is only used to identify trends and make the necessary predictions to assess whether the micro data follows the trends dictated by the theory and checked by experiment.

For the engaged setting, the data also shows a good correlations that follows the expected trends. For the macro version, the natural frequency can be assessed to be around  $130 \pm 24.7$  Hz, with a significant deviation shown by the first two data sets. The decrease in the accuracy can be attributed to the lumped stiffness model and its correction using the effective mass. It is clear that the correction, in this case, made the data jump away from the expected range rather than bring it closer to it as in the unengaged case. The factor was calculated using FEA as before, which leads to the hypothesis that there is also a scaling factor associated with an effective stiffness as well as for the effective mass.

The stiffness calculations assumed that the connections between the flexures were rigid, an assumption that seems to not hold true in the engaged case. If that assumption is annulled, then looking back at **Eq. 13** and **Figure 1** it is obvious that the length of the connecting flexure must come into play in the definition of  $k_2$ . The length factor is inversely proportional to the stiffness which is proportional to the natural frequency, thus an increase in the length factor would correspond to a decrease in the stiffness and therefore a decrease in the natural frequency associated with it. This is what needs to happen for the lumped stiffness model's predictions to hold true, and therefore follow the trend that is specifically presented in the FEA analysis. Taking into account, therefore, the experimental and FEA data sets only, the natural frequency for the macro device is clearly  $130 \pm 2.44$  Hz. This second value is much closer to the expected natural frequency of the macro device, the slight increase over the unengaged version being attributed to the difference in the stiffness to mass ratio. The micro device in the engaged setting presents the same increasing trend as the unengaged setting. Once again, this can be attributed to an 'effective stiffness' fraction which would make the FEA data, as the more complete analysis, the most reliable. Nonetheless, a value of  $40 \pm 3.7$  kHz can be estimated for the micro engaged device.

Upon further consideration of the natural frequencies for each of the normal directions of vibration, a surprising trend appears. Implicitly stated in **Table 2** is the fact that both the engaged and unengaged settings of the macro device share the same natural frequency ranges. Although unexpected during the period of data acquisition, this trend seems to agree with the above discussion of the effective stiffness factor. Although the stiffness increases substantially once Flexure 2 is engaged, as does the effective vibrating mass, there seems to be some sort of extra factor associated with this setting that scales the expected natural frequency down to a value similar to that seen in the unengaged case. This prospect is clear in **Figure A4.3** where experimental trends are plotted and averaged.

## 6.0 Conclusion

This study looked to find the natural harmonic frequencies of a tunable stiffness in-plane AFM probe. The dynamic behavior of the three primary modes of vibration were identified through analysis and. The natural frequencies for the micro scale version of the probe were found to be 81.314 kHz, 51.438 kHz, and 54.899 kHz for the X, Y, and Z directions of vibration respectively. The error associated with these measurements is approximately 3-4 kHz according to the macro scale experimental data scaling. This would correspond to an average percent error of 6.6% for the micro scale. Although it is surprising that such a large percent error would be associated with a purely computational approach to identifying the natural frequencies, it is not as daunting as it would seem. The micro scale case is unforgiving regarding small deviations and any slight inconsistency will be amplified to an error reading in this range.

This dynamic analysis of the tunable stiffness probe is very basic in its scope. The immediate next step in this project will be to conduct a vibration test on the micro probe itself to see if the predicted frequencies correlate with the ones exhibited by the physical device. If that experiment yields satisfactory results, a full dynamic spectrum analysis should be performed to assess whether the assumptions associated with the modal analysis hold true. This more involved experimental analysis will include a setup like the one shown in **Figure 15** where a position sensor (resistive or capacitive) is connected to the AFM probe to accurately map its motion.

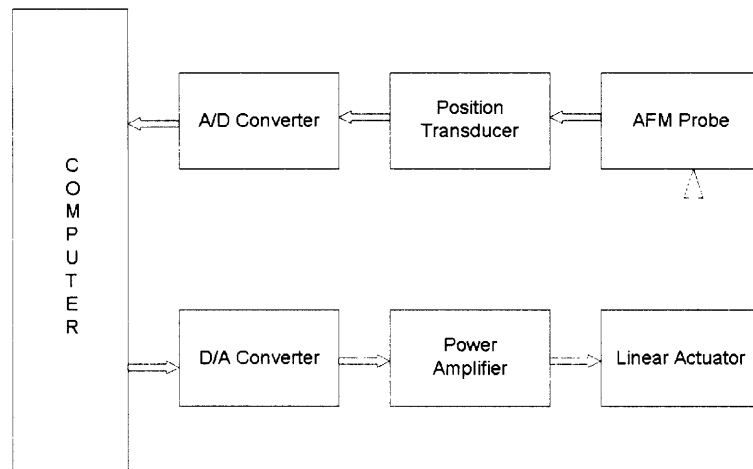


**Figure 15:** Experimental Setup Schematic for Full Dynamic Spectrum Testing

Further computational analyses should also be pursued to evaluate the effective stiffness hypothesis that was quoted as the reason for the engaged setting to exhibit a slightly different trend than the unengaged setting.

## References:

- [1] Paulapuro, H. (2002). *Research Equipment* [online]. Helsinki University of Technology, Paper Technology. Available from: <http://tkk.fi/Units/Paper/images/afm.jpg> (Accessed 09 April 2005)
- [2] Mueller-Falcke, C., Song, Y. A., Kim, S. G. 'Tunable Stiffness Scanning Microscope Probe', *Proceedings of SPIE*, **5604**, 31, Philadelphia, PA, October 2004.
- [3] Mueller-Falcke, C., Gouda, S. D., Kim, S., Kim, S. G. (2005), 'A Nanoscanning Platform for Bio Engineering', *First International Conference on Bio-Nano-Informatics (BNI) Fusion*, July 2005, Marina del Rey, CA.
- [4] Li, H. Q., (24 April 1997), *Atomic Force Microscopy* [online], University of Guelph, Department of Chemistry. Available from: <http://www.chembio.uoguelph.ca/educmat/chm729/afm/firstpag.htm> (Accessed 21 April 2005)
- [5] Palm, W. J. III (1983), *Modeling, Analysis and Control of Dynamic Systems*, New York, John Wiley & Sons. (ISBN 0-471-05800-9)
- [6] Parente, Peter (2002), *The Discrete Fourier Transform* [online], University of North Caroline, Chapel Hill, Department of Computer Science. Available from: [http://cs.unc.edu/~parente/igv/hw3/parente\\_hw3.html](http://cs.unc.edu/~parente/igv/hw3/parente_hw3.html) (Accessed 17 March 2005).
- [7] Hunter, I. (2003). 2.671 *Measurement and Instrumentation*, 'Fourier Transform', Department of Mechanical Engineering, MIT.
- [8] Hunter, I. (2003). 2.671 *Measurement and Instrumentation*, 'Fast Fourier Transform', Department of Mechanical Engineering, MIT.
- [9] Bracewell, R. N. (1986), *The Fourier Transform and Its Applications: Second Edition, Revised*, New York, McGraw Hill Book Company. (ISBN 0-07-007015-6)

## Appendices:

### A1. ANSYS code

#### A1.1 ANSYS code for micro device: unengaged

```
/AUX15
IOPTN.IGES.NODEFEAT
!*
IOPTN.MERGE.YES
IOPTN.SOLID.YES
IOPTN.SMALL.YES
IOPTN.GTOLER, DEFA
IGESIN,'trimmedsimple',igs',C:\Temp\'
VPLOT
!*
FINISH
/PREP7
!*
ET,1,SOLID92
!*

MPTEMP,.....
MPTEMP,1,0
MPDATA,EX,1,..,4.02E-3
MPDATA,PRXY,1,..,22
MPTEMP,.....
MPTEMP,1,0
MPDATA,DENS,1,1,200E-15
SMRT,6
MSHAPE,1,3D
MSHKEY,0
!*
CM,_Y,VOLU1
VSEL,,,1
CM,_Y1,VOLU
CHKMSH,'VOLU'
CMSEL,S,_Y
!*
VMESH,_Y1
!*
CMDELE,_Y
CMDELE,_Y1
CMDELE,_Y2
!*
FINISH
/SOL
!*
ANTYPE,2
!*
MSAVE,0
!*
MODOPT,LANB,10
EQSLV,SPAR
MXPAND,10,..,0
LUMPM,0
PSTRES,0
!*
MODOPT,LANB,10,1,10000, .OFF
FLST,2,3,5,ORDE,2
FITEM,2,104
FITEM,2,-106
!*
/GO
DA,P51X,ALL,
/STATUS,SOLU
SOLVE
```

## A1.2 ANSYS code for micro device: engaged

```
/AUX15
IOPTN,IGES,NODEFEAT
!*
IOPTN,MERGE,YES
IOPTN,SOLID,YES
IOPTN,SMALL,YES
IOPTN,GTOI,ER,DEFA
IGESIN,'trimmedengaged',igs,'C:\Temp\'
VPLOT
!*
FINISH
/PREP7
!*
ET,1,SOLID92
!*
MPTEMP,.....
MPTEMP,1,0
MPDATA,EX,1,4.02E-3
MPDATA,PRXY,1,22
MPTEMP,.....
MPTEMP,1,0
MPDATA,DENS,1,1.200E-15
SMRT,6
MSHAPE,1,3D
MSHKEY,0
!*
CM,_Y,VOLU
VSEL,,,1
CM,_Y1,VOLU
CHKMSH,'VOLU'
CMSEL,S,_Y
!*
VMESH,_Y1
!*
CMDELE,_Y
CMDELE,_Y1
CMDELE,_Y2
!*
FINISH
/SOL
!*
ANTYPE,2
!*
MSAVE,0
!*
MODOPT,LANB,10
EQLV,SPAR
MXPAND,10,1,0
LUMPM,0
PSTRES,0
!*
MODOPT,LANB,10,1,10000,.OFF
FLST,2,3,5,ORDE,2
FITEM,2,155
FITEM,2,-157
!*
/GO
DA,P51X,ALL,
/STATUS,SOLU
SOLVE
```

## A2. ANSYS Outputs: Mode Shapes



**Figure A2.1:** Unengaged Micro Device Mode Shapes (as plotted by ANSYS's postprocessor)

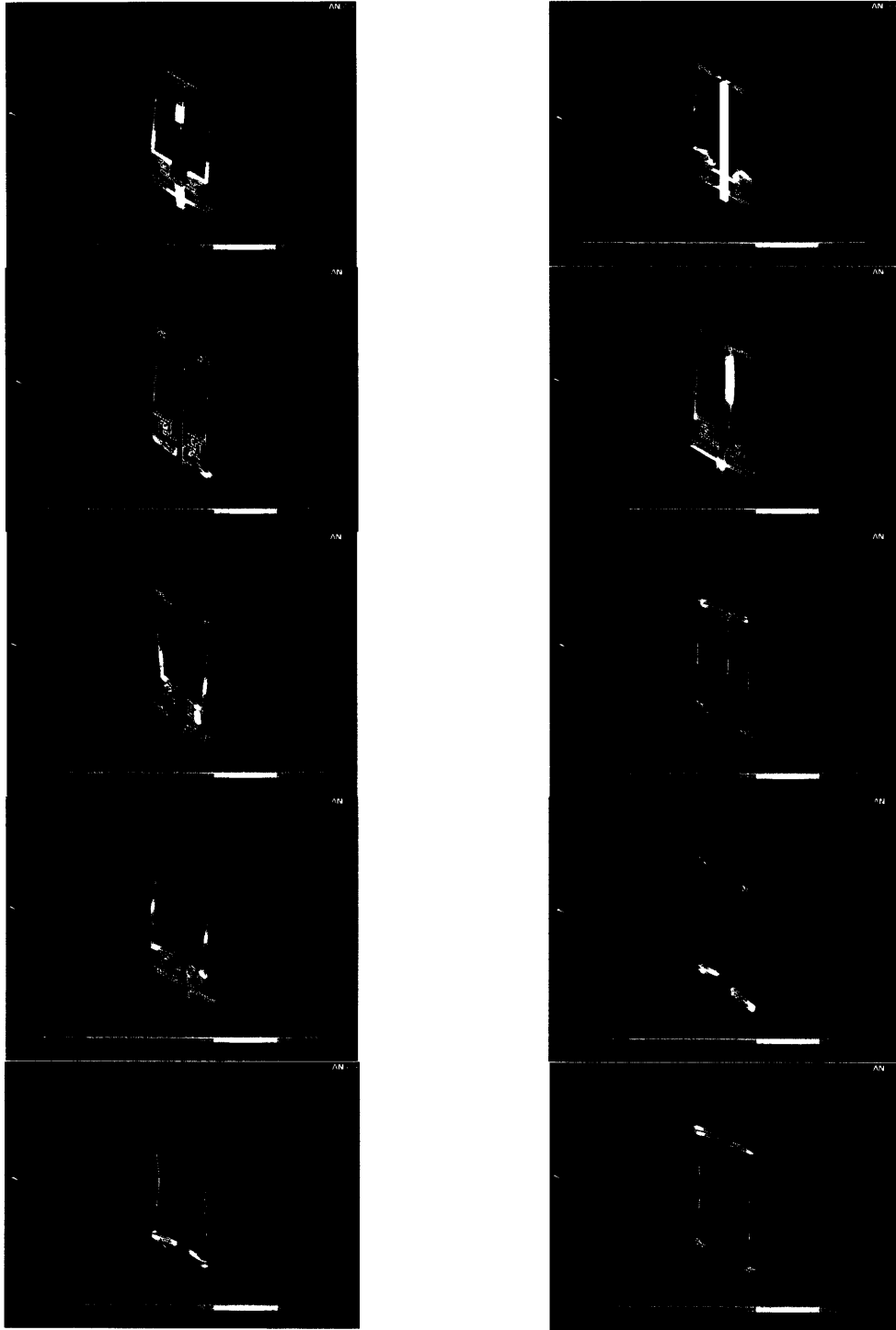


**Figure A2.2:** Engaged Micro Device Mode Shapes (as plotted by ANSYS's postprocessor)

### A3. MATLAB code

#### A3.1 MATLAB script for video data

```
"MATLAB CODE FOR CALCULATION OF THE DUSSES PERIOD"  
"A3.1.1"  
  
clear all; close all;  
  
C = 10; % constant of spring constant  
ES = 119E-6; % elastic strain rate (m/s)  
  
% Material properties: Young's Modulus (E) and Poisson's Ratio (nu)  
E = 200000; % Young's Modulus (N/m^2)  
nu = 0.3; % Poisson's Ratio  
  
% Geometric Properties: Area (A) and Moment of Inertia (I)  
A = 0.0001; % Area (m^2)  
I = 1e-10; % Moment of Inertia (m^4)  
  
% Damping Properties: Damping Coefficient (D) and Damping Ratio (zeta)  
D = 0.001; % Damping Coefficient (N/m)  
zeta = 0.05; % Damping Ratio  
  
% Natural Frequency (omega_n) and Damped Frequency (omega_d)  
omega_n = sqrt(E/I); % Natural Frequency (rad/s)  
omega_d = omega_n * sqrt(1 - zeta^2); % Damped Frequency (rad/s)  
  
% Time Constants: Time to Peak (TST) and Time to Settle (TSO)  
TST = 1/omega_n; % Time to Peak (s)  
TSO = 4/TST; % Time to Settle (s)  
  
% Damped Time Constants: Damped Time to Peak (DTST) and Damped Time to Settle (DTSO)  
DTST = 1/omega_d; % Damped Time to Peak (s)  
DTSO = 4/DTST; % Damped Time to Settle (s)  
  
% Frequency Constants: Frequency to Peak (FST) and Frequency to Settle (FSO)  
FST = C ./ DTST; % Frequency to Peak (Hz)  
FSO = C ./ DTSO; % Frequency to Settle (Hz)  
  
% "Elastic Strain Rate"  
EA1 = A1+ES;  
EA2 = A2+ES;  
  
EB1 = B1-ES;  
EB2 = B2-ES;  
  
EDTST = EB1 + (EA1.*-1); % Damped Time to Peak (s)  
EDTSO = EB2 + (EA2.*-1); % Damped Time to Settle (s)  
  
EFST = C ./ EDTST; % Frequency to Peak (Hz)  
EFSTO = C ./ EDTSO; % Frequency to Settle (Hz)  
  
% "Elastic Strain Rate"  
MEA1 = A1-ES;  
MEA2 = A2-ES;  
  
MEB1 = B1+ES;  
MEB2 = B2+ES;  
  
MEDTST = MEB1 + (MEA1.*-1); % Damped Time to Peak (s)  
MEDTSO = MEB2 + (MEA2.*-1); % Damped Time to Settle (s)  
  
MEFST = C ./ MEDTST; % Frequency to Peak (Hz)
```

```

MEFSO = C ./ MEDTSO; % Natural frequency
% Plotting the results
figure(1);
plot(RSO ,FSO , RSO, MEFSO, RSO, EFSO, RSO, [(ASO+SSO) (ASO+SSO) (ASO+SSO) (ASO+SSO)],
RSO,[(ASO-SSO) (ASO-SSO) (ASO-SSO) (ASO-SSO)] , RSO, [ASO ASO ASO ASO]);
xlabel('Time (sec)'); ylabel('Frequency (Hz)'); title('Frequency spectra: Soft -trial');

hold on;
figure(2);
% Plotting the results
plot(RSO ,FST , RSO, MEFSO, RSO, EFST, RSO, [(AST+SST) (AST+SST) (AST+SST) (AST+SST)],
RSO,[(AST-SST) (AST-SST) (AST-SST) (AST-SST)] , RSO, [AST AST AST AST]);
xlabel('Time (sec)'); ylabel('Frequency (Hz)'); title('Frequency spectra: Hard -trial');

```

### A3.2 MATLAB script for lumped stiffness model

```

% Parameters
% Material properties
E = [2.34E9; 4.02E9; 4.02E9]; % Young's modulus (N/m^2)
w = [.005555625; .020066; 2.0066E-5]; % Weight (kg)
L = [.0315; .180086; 1.80086E-4]; % Length (m)
L1 = [.020916; .145034; 1.45034E-4]; % Length (m)
L2 = [.0133962; .089916; 8.9916E-5]; % Length (m)
L3 = [.02677916; .1651; 1.651E-4]; % Length (m)
t = [.00208; .009906; 9.906E-6]; % Thickness (m)

m = [.10812*.167198 .11599*.73417 ; 5.78551761*.167198 6.47311647*.73417 ;
5.78551764E-9*.129706 6.47311668E-9*.192473]; % Mass (kg)
% Stiffness
k1 = (2.*E.*w.*(t.^3))./(L.^3 + 2.*(L1.^3)); % Stiffness (N/m)
k2 = (2.*E.*w.*(t.^3))./(L2.^3); % Stiffness (N/m)
k3 = (E.*w.*(t.^3))./(L3.^3); % Stiffness (N/m)

K = [k1+k3 k1+k2+k3]; % Stiffness matrix (N/m)

SWN = [K./m]; % Natural frequency (rad/s)
WN = sqrt(SWN); % Natural frequency (Hz)
Wn = WN./(2*3.14159); % Natural frequency (Hz)

```

### A3.3 MATLAB script for results summary

```

% Parameters
% Material properties
clear all; close all;
A = [1:1:5]; % Natural frequency (rad/s)
B = [1:1:3]; % Natural frequency (Hz)

```

```

WnLU = [49.423 120.26 116.03 120.84 121.31];  natural frequency-undamped length [Hz]
WnLE = [154.12 178.95 130.04 132.03 127.16];  natural frequency-undamped length [Hz]

WnSU = [11566 28287 32115.71];  natural frequency-damped length [Hz]
WnSE = [31044 36231 70761];  natural frequency-damped length [Hz]

WNLU = 105.5736;  average natural frequency-undamped length [Hz]
WNLE = 144.46;  average natural frequency-undamped length [Hz]

STLU = std(WnLU);  standard deviation-undamped length [Hz]
STLE = std(WnLE);  standard deviation-undamped length [Hz]

TELU = [WNLU+STLU WNLU+STLU WNLU+STLU WNLU+STLU WNLU+STLU];  upper bound natural frequency
BELE = [WNLU-STLU WNLU-STLU WNLU-STLU WNLU-STLU WNLU-STLU];  lower bound natural frequency

TELE = [WNLE+STLE WNLE+STLE WNLE+STLE WNLE+STLE WNLE+STLE];
BESE = [WNLE-STLE WNLE-STLE WNLE-STLE WNLE-STLE WNLE-STLE];

WNSU = 23989.57;  average natural frequency-damped length [Hz]
WNSE = 46012;  average natural frequency-damped length [Hz]

STSU = std(WnSU);  standard deviation-damped length [Hz]
STSE = std(WnSE);  standard deviation-damped length [Hz]

TESU = [WNSU+STSU WNSU+STSU WNSU+STSU];
BESU = [WNSU-STSU WNSU-STSU WNSU-STSU];

TESE = [WNSE+STSE WNSE+STSE WNSE+STSE];
BESE = [WNSE-STSE WNSE-STSE WNSE-STSE];

figure(1);
plot(A, WnLE, A, [144.46 144.46 144.46 144.46 144.46], A, TELE, A, BESE );
xlabel('Natural Frequency [Hz]'); ylabel('Natural Frequency [Hz]');
title('Average Natural Frequency-Undamped Length');

figure(2);
plot(A, WnLU, A, [105.5736 105.5736 105.5736 105.5736 105.5736], A, TELU, A, BELE);
xlabel('Natural Frequency [Hz]'); ylabel('Natural Frequency [Hz]');
title('Average Natural Frequency-Undamped Length');

figure(3);
plot(B, WnSE, B, [46012 46012 46012], B, TESE, B, BESE);
xlabel('Natural Frequency [Hz]'); ylabel('Natural Frequency [Hz]');
title('Average Natural Frequency-Damped Length');

figure(4);
plot(B, WnSU, B, [23989.57 23989.57 23989.57], B, TESU, B, BESU);
xlabel('Natural Frequency [Hz]'); ylabel('Natural Frequency [Hz]');
title('Average Natural Frequency-Damped Length');

```

## A4. Experiment Outputs

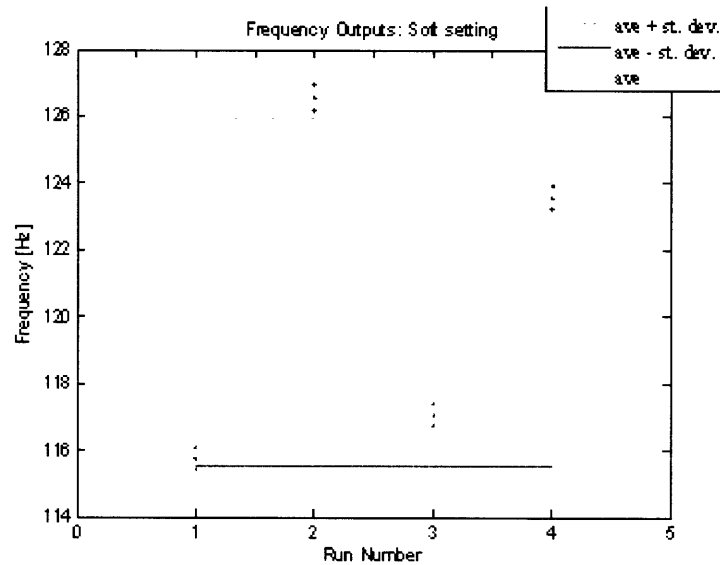


**Figure A4.1:** Frequency Outputs from Video Capture: Unengaged macro device

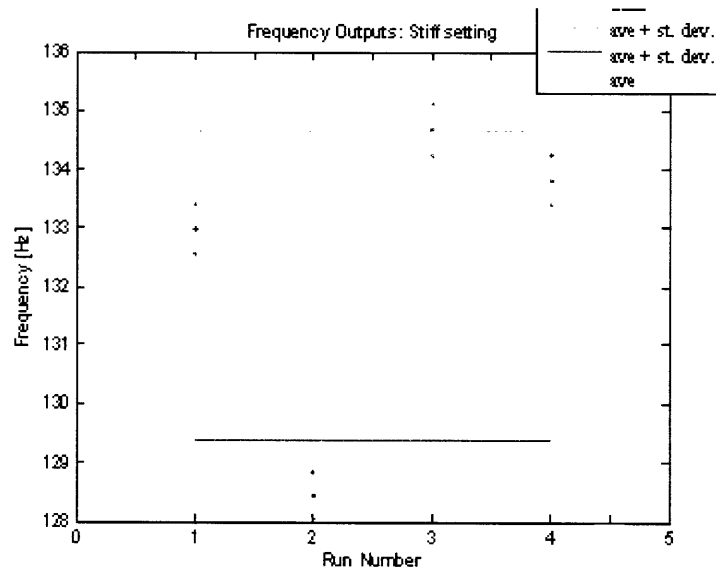


**Figure A4.2:** Frequency Outputs from Video Capture: Engaged macro device

These two figures present the frequency calculated from the Phantom high speed camera output. The blue dots indicate the calculated frequency using [Eq. 17](#). Because of the camera tolerance, the red and green markers show the ‘error envelope’ that represents the range in which the actual value is likely to be in. The average natural frequency of the data sets was then calculated and is represented by the olive line. The blue and magenta lines correspond to one standard deviation above and below the average.

The numerical values for all these parameters are:

**Table A4.1:** Numerical values for Frequency Outputs from Video Capture

	$f_1$ [Hz]	$f_2$ [Hz]	$f_3$ [Hz]	$f_4$ [Hz]	Frequency Tolerance	Average [Hz]	Standard Deviation
<b>Engaged</b>	132.96	128.43	134.67	133.81	119 $\mu$ s	132.03	2.63
<b>Unengaged</b>	115.75	126.56	117.04	125.58	119 $\mu$ s	120.73	5.18

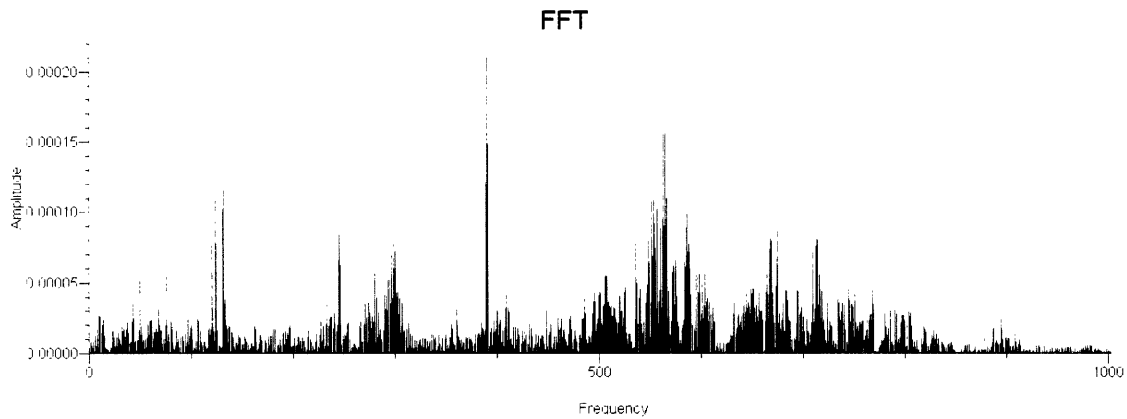


**Figure A4.3:** Fast Fourier Transform of the Unengaged Macro Probe where each spike in the spectrum represents a natural frequency in one of the main directions of motion.

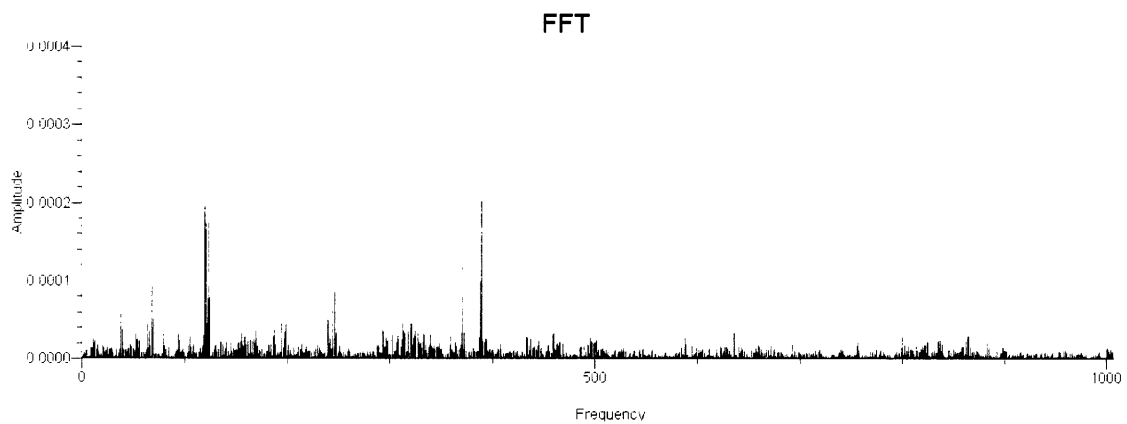


**Figure A4.4:** Fast Fourier Transform of the Engaged Macro Probe where each spike in the spectrum represents a natural frequency in one of the main directions of motion.

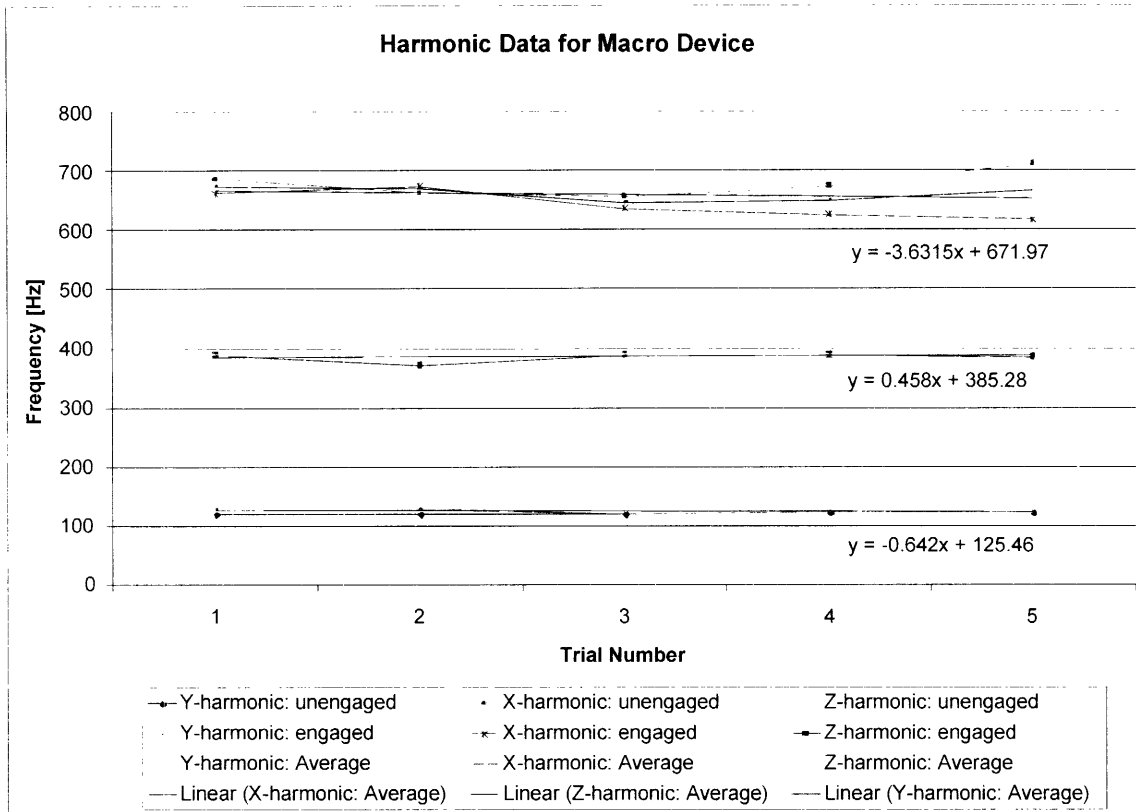


**Figure A4.5:** Natural Frequency Experimental Data: Average of the Sound and HSV Camera outputs



Room 14-0551  
77 Massachusetts Avenue  
Cambridge, MA 02139  
Ph: 617.253.5668 Fax: 617.253.1690  
Email: docs@mit.edu  
<http://libraries.mit.edu/docs>

## **DISCLAIMER OF QUALITY**

Due to the condition of the original material, there are unavoidable flaws in this reproduction. We have made every effort possible to provide you with the best copy available. If you are dissatisfied with this product and find it unusable, please contact Document Services as soon as possible.

Thank you.

**Some pages in the original document contain color pictures or graphics that will not scan or reproduce well.**